



**HAL**  
open science

## Effect of methylene blue on the formation of oxidized phospholipid vesicles

Jean-François Fabre, Muriel Cerny, Audrey Cassen, Zéphirin Mouloungui

► **To cite this version:**

Jean-François Fabre, Muriel Cerny, Audrey Cassen, Zéphirin Mouloungui. Effect of methylene blue on the formation of oxidized phospholipid vesicles. 2020. hal-03037371

**HAL Id: hal-03037371**

**<https://hal.science/hal-03037371>**

Preprint submitted on 16 Dec 2020

**HAL** is a multi-disciplinary open access archive for the deposit and dissemination of scientific research documents, whether they are published or not. The documents may come from teaching and research institutions in France or abroad, or from public or private research centers.

L'archive ouverte pluridisciplinaire **HAL**, est destinée au dépôt et à la diffusion de documents scientifiques de niveau recherche, publiés ou non, émanant des établissements d'enseignement et de recherche français ou étrangers, des laboratoires publics ou privés.



Distributed under a Creative Commons Attribution - NonCommercial - NoDerivatives 4.0 International License







## Open Archive Toulouse Archive Ouverte (OATAO)

OATAO is an open access repository that collects the work of Toulouse researchers and makes it freely available over the web where possible

This is a Publisher's version published in: <http://oatao.univ-toulouse.fr/24613>

**Official URL:** <https://doi.org/10.1101/403634>

**To cite this version:**

Fabre, Jean-François  and Cerny, Muriel  and Cassen, Audrey  and Mouloungui, Zéphirin  *Effect of methylene blue on the formation of oxidized phospholipid vesicles.* (2018) bioRxiv. 1-32. ISSN 2692-8205

Any correspondence concerning this service should be sent to the repository administrator: [tech-oatao@listes-diff.inp-toulouse.fr](mailto:tech-oatao@listes-diff.inp-toulouse.fr)

## **Effect of methylene blue on the formation of oxidized phospholipid vesicles**

*J-F. Fabre, M. Cerny, A. Cassen, Z. Mouloungui*

1 **Abstract**

2 Soybean phosphatidylcholine, which is rich in linoleic acid, was oxidized with singlet oxygen  
3 through photosensitization with methylene blue. This compound facilitates the oxidation of  
4 phospholipids relative to the reaction with free unsaturated fatty acids. A response surface  
5 methodology was used to control oxidation, with methylene blue concentration and the  
6 amount of available air as independent variables. The conjugated diene-to triene ratio was  
7 then monitored. Hydroperoxide yield dependent principally on the amount of air, whereas  
8 photosensitizer concentration strongly influenced the size and zeta potential of vesicles  
9 formed by the sonication of oxidized phospholipids in water. Methylene blue plays an  
10 important role in the surface charge expression and ion permeability of these vesicles.

11 Keywords: Methylene blue, phospholipids, singlet oxygen, oxidation, liposomes, zeta  
12 potential, permeability, soybean

13

## 14           **1. Introduction**

15   Phospholipids were initially considered to be a by-product of oil refining. However, over  
16   time, these amphipathic molecules have become essential components of food, cosmetic and  
17   pharmaceutical formulations. Their organization as liposomes in water confers considerable  
18   added value for drug encapsulation and delivery(1–3). The size, shape and permeability of  
19   liposomes depend strongly on the nature and composition of the phospholipids they contain.  
20   For example, liposomes formed with phosphatidylcholine (PC), the most abundant  
21   phospholipid in animals and plants, are generally larger than those formed with  
22   phosphatidylethanolamine(4). The nature of the fatty acids is also of great importance.  
23   Saturated fatty acids form more compact membranes that are generally less permeable for  
24   some compounds than the equivalent unsaturated fatty acids(5–7) but, for some ions, the  
25   membranes formed with unsaturated fatty acids are less permeable than those formed with  
26   saturated fatty acids(8). Long fatty acid chains generally result in lower permeability to  
27   ions(9, 10). Phospholipid oxidation, which occurs at double bonds, can have several effects.  
28   Oxidation can stimulate lipid flip-flop within the membrane(11,12), and oxidized liposomes  
29   are generally considered more permeable to water (13,14), glucose(15) and dextran(16). High  
30   levels of oxidation can also lead to pore formation (17,18,19), and membrane disruption,  
31   mostly due to the presence of shortened carboxyacyl units (20), as hydroperoxides cause less  
32   damage. However, all these features are heavily dependent on the nature and concentration of  
33   the oxidized compounds and it is thus essential to control oxidation, to modify the hydrophilic  
34   and permeation properties of these liposomes as desired. Soybean seeds are one of the most  
35   widely used sources of commercial phospholipids. Phosphatidylcholine is the principal  
36   soybean phospholipid. Its fatty acid chains are mostly unsaturated (oleic, linoleic, linolenic  
37   acids), making it a good model for oxidation studies. A number of different methods are  
38   available for oxidizing soybean phospholipids(21, 22) but the use of singlet oxygen is a  
39   simple and powerful approach. This method generally involves the disproportionation of  
40   hydrogen peroxide to generate singlet oxygen, and the use of molybdate as a catalyst (23, 24).

41 However, a photosensitizer can also be used, and this method is often used with fatty acids or  
42 phospholipids. Various dyes can be used for this purpose, including protoporphyrin IX (25),  
43 rose bengal (26), pheophorbide (27) and methylene blue (MB), one of the most widely used  
44 photosensitizers (28–32). Under illumination, the methylene blue cation reaches an excited  
45 singlet state. As a conjugated dye containing a single sulfur as a ring heteroatom, it can  
46 undergo efficient intersystem crossing to reach a triplet state with a relatively long lifetime.  
47 Photooxidation can then occur through two possible mechanisms. In type II mechanisms,  
48 triplet oxygen reacts with MB through an energy transfer process to form singlet oxygen,  
49 while the methylene blue returns to its fundamental level (33, 34). Singlet oxygen, which is  
50 highly electrophilic, generates hydroperoxides on reaction with unsaturated chains. In type I  
51 mechanisms, MB reacts with the substrate via electron transfer to form radicals.  
52 Hydroperoxides are generally formed first, through a type II mechanism, which is then  
53 followed by a type I mechanism (35). However, the contribution of methylene blue is often  
54 limited to the production of singlet oxygen, and this compound is generally removed from the  
55 reaction medium for the purification of oxidized products. To our knowledge, its possible  
56 contribution to the formation and properties of vesicles has hardly been explored.

## 57 **2. Materials and methods**

58 Methylene blue trihydrate, linoleic acid (>99%), linolenic acid (>99%), and oleic acid (99%),  
59 for use as analytical reactants and standards, were purchased from Sigma Aldrich (St Quentin  
60 Fallavier, France). Soybean lecithin (ca. 90% phosphatidylcholine) was purchased from VWR  
61 (Fontenay sous Bois, France). Dilinoleylphosphatidylcholine (>99%) was purchased from  
62 COGER (Paris, France)

### 63 **Chemical analysis**

64 The fatty acid profile of the phospholipids was determined after *trans*-methylation with  
65 TMSH (0.2 M trimethylsulfonium hydroxide in methanol) according to AFNOR Method NF  
66 EN ISO 12966-3. The fatty acid methyl esters (FAME) obtained by this transesterification

67 reaction were analyzed with a gas chromatograph (36) equipped with a CP-select CB column  
68 (50 m long, 0.32 mm i.d., 0.50  $\mu\text{m}$  film thickness); helium was used as the carrier gas, at a  
69 flow rate of 1.2 mL/minute; the split injector (1:100) and FID were maintained at 250°C ; the  
70 initial oven temperature was set to 185°C for 40 minutes, increased to 250°C at a rate of  
71 15°C/minute and maintained at this temperature for 10 minutes.

72 NMR experiments were carried out on a Bruker AVANCE III HD NMR spectrometer  
73 operating at 500.13 MHz for 1 h. This machine was equipped with a 5 mm BBFO ATMA  
74 Prodigy cryoprobe. This cryoprobe enhances the probe sensitivity at room temperature by a  
75 factor of 2 to 3 for X-nuclei from  $^{15}\text{N}$  to  $^{31}\text{P}$ . NMR experiments were recorded at 298 K,  
76 with the zgig30 pulse sequence. The recycle delay was adjusted to 2 s and the number of  
77 scans was set to 16. Topspin 3.2 software was used for data acquisition and processing in all  
78 NMR experiments.

79 The conjugated dienes and trienes generated by phospholipid oxidation were characterized by  
80 spectrophotometry with a SHIMADZU UV1800 spectrophotometer, in quartz cuvettes. The  
81 reference cuvette contained absolute ethanol. The contribution of methylene blue to the  
82 absorbances at 233 nm and 290 nm was ignored.

### 83 **Photosensitization**

84 Solutions of different concentrations of methylene blue in absolute ethanol were prepared in  
85 amber bottles and stored in the dark. Phospholipids were dissolved in these solutions at a  
86 concentration of 20 mg/mL, and the resulting solutions were illuminated for eight hours in 20  
87 mL glass tubes (diameter: 15 mm) with an ATLAS SUNTEST CP+ device equipped with a  
88 1500 W xenon lamp simulating a spectral distribution close to that of natural sunlight.

### 89 **Size and zeta potential measurements**

90 The size and zeta potential of phospholipid vesicles were analyzed with a NANOSIZER ZS  
91 granulometer (Malvern). A 1 mL sample of the 20 mg/mL phospholipid solution in absolute

92 ethanol was dried under nitrogen. The resulting film was diluted in 2 mL of distilled water  
93 and sonicated for 3 minutes with a laboratory ultrasound probe (SONICS VIBRACELL -500  
94 equipped with a 3mm diameter probe, pulsation mode : 5 s ON/10 s OFF, amplitude: 57  
95  $\mu\text{m}/20\%$ ). The temperature was allowed to stabilize at 25°C for one minute, and  
96 measurements were performed three times, considering a refractive index for the lipid bilayer  
97 of 1.45 (37) and an absorption factor of 0.001. A backscattering detector was positioned at  
98 173°. Zeta potential values were obtained by correlating mobility measurements with the  
99 Smoluchowsky model.

## 100 **Permeation studies**

101 If the solute concentration differs between the phase within vesicles and the external phase,  
102 then there is an osmotic pressure exerts at both sides. Vesicles may undergo water or salt  
103 permeation to equilibrate this pressure. If selective, this permeation leads to a change in  
104 volume. For example, volume decreases if the vesicle rejects water to increase its internal  
105 solute concentration, or increases if the vesicle accepts water to decrease its internal solute  
106 concentration. Absorbance measurements are a good tool for measuring such changes,  
107 provided that they occur rapidly. Indeed, the absorbance of a stable dispersed medium is  
108 highly dependent on the refractive index of the dispersed particles, their concentration and  
109 their size. For a given refractive index and vesicle concentration, the change in absorbance is  
110 related to changes in size and, thus, to the exchanges of water and solutes between the  
111 vesicles and the surrounding medium.

112 According to Mie theory of light scattering (38), for a given refractive index, solutions of  
113 nanometric particles (10-100 nm) scatter much less light than solutions of micrometric  
114 particles, and have a lower light extinction value. The initial absorbance of vesicle solutions  
115 (before the occurrence of osmotic changes) may, therefore, be directly linked to vesicle size.  
116 It is difficult to measure absorbance at the precise time at which the vesicle suspension is  
117 dispersed in the medium. The absorbance reached at equilibrium (or at infinite time) is



118 therefore more usually measured. This approach also has the advantage that the delayed  
119 absorbance variation generally reflects a more precise equilibration of osmotic pressures.  
120 Decreases in absorbance have generally been linked to a global swelling, whereas shrinkage is  
121 accompanied by an increase in absorbance (6, 39).

122 The variation of absorbance can be modeled with an exponential law (see supporting  
123 information):

$$124 \quad A = A_{\text{inf}} + \Delta A \cdot \exp(-k \cdot t)$$

125 Where  $A_{\text{inf}}$  is the absorbance at infinite time,  $\Delta A$  is the change in absorbance between the  
126 initial measurement and infinite time, and  $k$  is a constant.

127 The swelling and shrinkage of phospholipid structures in hypertonic solutions were, therefore,  
128 measured with a Spectrostar NANO spectrophotometer, at a fixed temperature of 25°C, in  
129 polypropylene cuvettes. Kinetic measurements of extinction at 400 nm were performed at  
130 five-second intervals.

### 131 **Response surface methodology**

132 The experiment was designed and analyzed with NEMRODW 2000 (Mathieu D, Nony J,  
133 Phan-Tan-Luu R. NEMROD-W software. LPRAI; Marseille: 2000).

134 The experimental values were regressed with a second-order polynomial model:

$$135 \quad Y_k = b_0 + \sum_i b_i X_{i,k} + \sum_i b_{ii} X_{i,k}^2 + \sum_i \sum_{j \neq i} b_{ij} X_{i,k} X_{j,k}$$

136 Where  $Y_k$  is the calculated response value in the  $k^{\text{th}}$  experiment,  $X_{i,k}$  is the coded variable  $i$  for  
137 the  $k^{\text{th}}$  experiment,  $b_0$  is the intercept term,  $b_i$  is the main coefficient for each variable,  $b_{ii}$  is the  
138 squared coefficient and  $b_{ij}$  is the interaction term. The pertinence of the model was assessed  
139 with the Fisher-Snedecor test, comparing model and residual variances, and its validity (or  
140 descriptive importance) was determined by comparing the residual and experimental  
141 variances (see supplementary information). A proba.1 value below 5 was considered to

142 indicate pertinence of the model (at a 95% confidence level). A proba.2 value below 5 was  
143 interpreted as indicating that the model did not describe the observed values (little chance that  
144 any deviation from the model could be explained by the experimental error). Measurements  
145 were also performed for test points, to assess the predictive value of the model in the  
146 experimental domain.

### 147 3. Results and Discussion

#### 148 3.1. Fatty acid distribution and oxidation

149 The fatty acid distribution of soybean phosphatidylcholine can be obtained both by  $^1\text{H}$  NMR  
150 analysis (40, 41) on intact phospholipids and by GC after transmethylation. NMR analysis is  
151 based on the different chemical shifts between the terminal methyl, allyl and alkene  
152 hydrogens of oleic, linoleic and linolenic acids. It is more difficult to determine the  
153 composition of saturated acids by this method, which is therefore used mostly to determine  
154 unsaturated fatty acid content. The two methods gave similar results for unsaturated fatty acid  
155 composition (table 1).

Fatty acid	% by GC	% by NMR
C16:0 – palmitate	$14.11 \pm 0.15$	<19
C18:0 – stearate	$3.85 \pm 0.13$	<5
C18:1 – oleate	$11.31 \pm 0.03$	13.7
C18:1n-7c – vaccenate	$1.66 \pm 0.06$	
C18:2n-6c – linoleate	$63.27 \pm 0.14$	59.5
C18:3 – linolenate	$5.80 \pm 0.05$	7.5

156 Table 1. Fatty acid distribution of soybean phosphatidylcholine according to GC and  $^1\text{H}$  NMR  
157 analyses

158 NMR cannot distinguish between oleate and vaccenate. The results obtained indicate that the  
159 principal fatty acids of soybean PC were linoleic, palmitic, then oleic and linolenic acids. The  
160 fatty acids of this molecule are, therefore, mostly polyunsaturated.

161 The oxidation of soybean PC was further investigated by preparing solutions of free linoleic,  
 162 linolenic, and oleic acids and soybean PC, at a concentration of 20 mg/mL, in absolute  
 163 ethanol. A 10 mL sample of each solution was poured into a 20 mL glass tube, which was  
 164 then hermetically sealed. The tube was then illuminated for 8 hours, and NMR analysis was  
 165 performed on the products. The oxidation of linoleic, linolenic and oleic acids was  
 166 characterized by the appearance of peaks (fig. 1) between 4 and 4.5 ppm (CH-OOH) , 5.4 and  
 167 6.5 ppm (conjugated double bonds) and 11 and 11.5 ppm (-OOH)(42,43,44), as shown in the  
 168 supplementary information.

169 The various hydroperoxide signals can be integrated to determine the formation yield. As for  
 170 fatty acids (table 2), similar integration results were obtained if we considered both hydrogens  
 171 of the hydroperoxide group (-CHOOH). The protons carried by the carbon in soybean  
 172 phospholipids are partially screened by peaks corresponding to the polar phosphocholine  
 173 moiety. Only the hydrogens corresponding to linoleic acid are visible. Integration is therefore  
 174 best performed with the hydrogen carried by the oxygen (-CHOOH).

175 Knowing the composition of the phospholipid tested, which consisted of 80% unsaturated  
 176 fatty acids, we can calculate that, if one hydroperoxide per unsaturated chain is considered,  
 177 the maximum amount of hydroperoxide in one molecule of phospholipid would be 1.6. For  
 178 soybean phospholipid, the hydroperoxide yield can, therefore, be expressed as:

179 
$$Y = \frac{100 \times INT(OOH)}{1.6}$$
 where INT(OOH) is the integration value for OOH/molecule.

Oxidized substrate	<u>CH</u> -OOH		<u>CH</u> -OO <u>H</u>		Yield
	Chemical shifts (ppm)	Integration	Chemical shifts (ppm)	Integration	$\frac{100 \times INT(OOH)}{MAX_{th}(OOH)}$
Oleic acid	4.04 , 4.09	0.14 , 0.02	11.2	0.14	14 %
Linoleic acid	<b>4.13 , 4.22</b>	0.05 , 0.05	11.2-11.4	0.12	12 %

Linolenic acid	4.03 – 4.30	0.14	11.3-11.4	0.14	14 %
Soy PC	<b>4.13, 4.22</b>	0.24 , 0.27	11.3-11.6	0.66	<b>40 %</b>

180 Table 2. Hydroperoxide yield according to <sup>1</sup>H NMR analysis

181 Yields were similar and low for the three unsaturated fatty acids (table 2), whereas soybean  
 182 phospholipid was much more oxidized. The oxidation of linoleic and linolenic acids can also  
 183 be monitored by spectrophotometry. Hydroperoxide generation leads to the formation of  
 184 conjugated double bonds the absorbance of which can be monitored over time. Conjugated  
 185 dienes absorb at 230-235 nm, whereas conjugated trienes absorb at 270-275 nm. The  
 186 absorbances of the phospholipid solutions were measured at different dilutions, to obtain the  
 187 extinction coefficient with the Beer-Lambert formula:

188  $A = \epsilon_n \cdot c_n \cdot l$  or  $A = \epsilon_m \cdot c_m \cdot l$  regardless of whether molar concentration or mass concentration is  
 189 considered.

190  $\epsilon_n$  is the molar extinction coefficient ( $L \cdot mol^{-1} \cdot cm^{-1}$ ),  $c_n$  is the molar concentration ( $mol \cdot L^{-1}$ ),  $l$   
 191 is the path length (cm) in the solution,  $\epsilon_m$  is the mass extinction coefficient ( $L \cdot g^{-1} \cdot cm^{-1}$ ), and  $c_m$   
 192 is the mass concentration ( $g \cdot L^{-1}$ ). For the comparison of molar extinction coefficients (table  
 193 3), an approximate molecular weight of 782 g/mol was chosen for soybean  
 194 phosphatidylcholine, corresponding to the molecular weight of dilinoleylphosphatidylcholine.

Oxidized substrate	$\epsilon_c$	$\epsilon_c$	Approx. $\epsilon_n$	Approx. $\epsilon_n$
	(233nm)	(270nm)	(233nm)	(270nm)
	( $L \cdot g^{-1} \cdot cm^{-1}$ )	( $L \cdot g^{-1} \cdot cm^{-1}$ )	( $L \cdot mol^{-1} \cdot cm^{-1}$ )	( $L \cdot mol^{-1} \cdot cm^{-1}$ )
Soy PC	5.88	0.19	4200	140
Linoleic acid	5.38	No peak	1450	No peak
Linolenic acid	7.94	0.9	1650	235

195 Table 3. Extinction coefficients of soybean PC and its polyunsaturated fatty acid constituents

196 Despite their similar hydroperoxide yields, oxidized linolenic acid had a higher extinction  
197 coefficient than linoleic acid at 233 nm, which can be explained by the larger number of  
198 unsaturated bonds, resulting in a larger number of positions at which conjugated dienes can be  
199 produced in linolenic (positions 9, 12, 13, 16) than in linoleic (positions 9 and 13) acids.  
200 Soybean phospholipid had a higher mass extinction coefficient than linoleic acid, and a molar  
201 extinction coefficient more than twice those of linoleic and linolenic acids. Its extinction  
202 coefficient at 270 nm was also less than half that of linolenic acid, with linolenic acid  
203 accounting for less than 10% of its composition. Soybean phospholipid is, thus, much more  
204 easily oxidized than its constitutive unsaturated fatty acids, consistent with the NMR results.  
205 Methylene blue may, therefore, have a higher affinity for phospholipids than for fatty acids.

### 206 **3.2. Response surface methodology**

207 Singlet oxygen production depends principally on the amount of photosensitizer and available  
208 triplet oxygen, provided that the samples are sufficiently illuminated. It was decided to work  
209 with air rather than pure oxygen, to obtain a procedure that was both simplified and scalable.  
210 For a constant temperature of 25°C, a change in the relative humidity of the air of less than  
211 10% during sample tube filling and a constant atmospheric pressure, the oxygen content of air  
212 can be considered stable and the amount of oxygen in the sample tubes is linearly correlated  
213 with the volume of available air. Using the highest illumination power available, >750 W/m<sup>2</sup>  
214 in the range 300-800nm, and limiting the duration of illumination to eight hours, the  
215 photosensitizer concentration and the volume of the sample solution in the sealed tube were  
216 varied, to modify the amount of air available. Phospholipid concentration was maintained at  
217 20 mg/mL. The aim was determine whether several valuable responses could be described  
218 qualitatively and/or quantitatively within a large domain of variations. Five values of log  
219 (1/V) were chosen for the volume (V) of the phospholipid solution, and three values of log(C)  
220 for the concentration of methylene blue.

221 A Doehlert matrix was used, with seven minimal experiments, two repetitions at the center of  
 222 the domain, one additional repetition and four test points at different coordinates (table 4).

EXP.	V (mL)	[MB] (mol.L <sup>-1</sup> )	LOG(1/V) real value	LOG ([MB]) real value	LOG(1/V) coded value X1	LOG ([MB]) coded value X2
1	2	1x10 <sup>-4</sup>	-0.3	-4	1	0
2	20	1x10 <sup>-4</sup>	-1.3	-4	-1	0
3	3.5	1x10 <sup>-3</sup>	-0.55	-3	0.5	0.866
4	11	1x10 <sup>-5</sup>	-1.05	-5	-0.5	-0.866
5	3.5	1x10 <sup>-5</sup>	-0.55	-5	0.5	-0.866
6	11	1x10 <sup>-3</sup>	-1.05	-3	-0.5	0.866
7	6	1x10 <sup>-4</sup>	-0.8	-4	0	0
8 repetition	6	1x10 <sup>-4</sup>	-0.8	-4	0	0
9 repetition	6	1x10 <sup>-4</sup>	-0.8	-4	0	0
10 repetition	11	1x10 <sup>-3</sup>	-1.05	-3	-0.5	0.866
11 test point	6	1x10 <sup>-3</sup>	-0.8	-3	0	0.866
12 test point	6	1x10 <sup>-5</sup>	-0.8	-4	0	-0.866
13 test point	15	1x10 <sup>-3</sup>	-1.18	-3	-0.76	0.866
14 test point	15	1x10 <sup>-5</sup>	-1.18	-5	-0.76	-0.866

223 Table 4. Extended Doehlert matrix for controlled singlet oxygen oxidation

224 An additional 6 mL sample of solution with a methylene blue concentration of 1x10<sup>-4</sup> M was  
 225 covered with a sheet of aluminum foil to block out the light as a control, and another control  
 226 consisted of methylene blue in ethanol alone. The color of these two control samples was  
 227 unchanged after 8 h in simulated sunlight, indicating that the methylene blue was not  
 228 degraded in these conditions. By contrast, the blue color of all the other samples in the  
 229 experimental design decreased, indicating a degradation of the methylene blue in the presence  
 230 of light, oxygen and phospholipids.

Exp.	X1	X2	Yield	Yield	$\epsilon_{233}$	$\epsilon_{233}$	$\epsilon_{233}/\epsilon_{270}$	$\epsilon_{233}/\epsilon_{270}$	Z	Z	$\zeta$	$\zeta$	$A_{inf}$	$A_{inf}$
			obs.	pred.	obs.	pred.	obs.	pred.	obs.	pred.	obs.	pred.	obs.	pred.
			%	%	L.g <sup>-1</sup> .cm <sup>-1</sup>	L.g <sup>-1</sup> .cm <sup>-1</sup>			nm	nm	mV	mV		
1	1	0	63.13	69.21	13.89	15.00	27.54	27.86	146	141	-0.03	-6.13	0.114	0.113
2	-1	0	26.25	20.17	5.20	4.10	15.96	15.64	338	342	4.08	10.18	0.409	0.410
3	0.5	0.866	60.63	54.55	15.91	14.81	16.17	15.85	126	130	5.24	11.34	0.138	0.193
4	-0.5	-0.866	30.63	36.71	4.54	5.65	28.59	28.91	523	518	2.54	-3.56	0.253	0.252
5	0.5	-0.866	43.13	43.96	6.74	5.64	27.71	27.39	308	312	2.55	8.65	0.190	0.191
6	-0.5	0.866	2.50	5.86	3.24	3.89	1.98	2.11	134	126	47.60	39.85	0.362	0.376

7	0	0	43.75	43.96	9.02	8.81	29.77	32.31	228	237	4.31	3.54	0.163	0.161
8	0	0	45.00	43.96	8.70	8.81	32.80	32.31	248	237	3.33	3.54	0.166	0.161
9	0	0	43.13	43.96	8.72	8.81	34.36	32.31	236	237	2.97	3.54	0.155	0.161
10	-0.5	0.866	3.13	5.86	3.44	3.89	1.91	2.11	122	126	38.20	39.85	0.391	0.376
<b>11</b>	<b>0</b>	<b>0.866</b>	<b>26.25</b>	<b>30.02</b>	<b>8.23</b>	<b>9.17</b>	<b>4.25</b>	<b>11.62</b>	<b>96</b>	<b>127</b>	<b>26.00</b>	<b>25.97</b>	<b>0.169</b>	<b>0.233</b>
<b>12</b>	<b>0</b>	<b>-0.866</b>	<b>40.00</b>	<b>36.70</b>	<b>6.21</b>	<b>5.46</b>	<b>29.71</b>	<b>30.79</b>	<b>284</b>	<b>414</b>	<b>-1.72</b>	<b>2.92</b>	<b>0.231</b>	<b>0.197</b>
<b>13</b>	<b>-0.76</b>	<b>0.866</b>	<b>0.63</b>	<b>-6.57</b>	<b>2.64</b>	<b>1.30</b>	<b>1.52</b>	<b>-4.93</b>	<b>122</b>	<b>126</b>	<b>42.50</b>	<b>46.77</b>	<b>0.546</b>	<b>0.470</b>
<b>14</b>	<b>-0.76</b>	<b>-0.866</b>	<b>16.25</b>	<b>36.86</b>	<b>2.72</b>	<b>5.89</b>	<b>20.06</b>	<b>25.85</b>	<b>360</b>	<b>573</b>	<b>-2.30</b>	<b>-7.23</b>	<b>0.414</b>	<b>0.300</b>

231 Table 5. Observed and predicted values for the various dependent variables measured.

### 232 3.2.1. Yield and extinction coefficients

233 The hydroperoxide yield for all experiments was determined by integrating the NMR signals  
 234 corresponding to hydroperoxide (-OOH). The analysis of variance yielded a Proba.1 value  
 235 <0.01, indicating that the regression was highly significant (confidence level of 99.9%).  
 236 However, a comparison of repeat experiments (table 5) revealed a small experimental error  
 237 that was insufficient to account for the difference between the experimental and calculated  
 238 values (Proba.2 =0.041). The model can provide qualitative information. An examination of  
 239 the different values of the experimental points (fig. 2a) and the correlation table (table 6)  
 240 clearly showed that yield was strongly dependent on the first factor,  $\log(1/V)$ .

	<i>X1</i>	<i>X2</i>												
	$\log(1/V)$	$\log(C)$	<i>Yield</i>	$\epsilon_{233nm}$	$\epsilon_{233nm}/\epsilon_{270nm}$	<i>Z average</i>	$\zeta$	$A_{inf}$						
<i>X1</i>	1													
<i>X2</i>	-0.06	1												
<i>Yield</i>	0.82	-0.31	1											
$\epsilon_{233nm}$	0.83	0.14	0.89	1										
$\epsilon_{233nm}/\epsilon_{270nm}$	0.44	-0.74	0.75	0.39	1									
<i>Z average</i>	-0.29	-0.85	0.09	-0.31	0.56	1								
$\zeta$	-0.38	0.76	-0.77	-0.45	-0.88	-0.60	1							
$A_{inf}$	-0.84	0.17	-0.87	-0.81	-0.63	0.03	0.56	1						

241 Table 6. Coefficients of correlation between different variables.

242 The best yields were obtained at intermediate concentrations of methylene blue and with low  
 243 solution volumes.

244 It was therefore important to determine whether monomer/dimer/trimer ratios were affected  
245 by high methylene blue concentrations. Several authors have suggested that dimer and trimers  
246 can be determined from different absorption bands. However, a UV/visible light spectrum  
247 analysis for different concentrations of the dye in ethanol (see supplementary information)  
248 showed that the ratios of absorption at 654 nm to absorption at 616 nm and 490 nm did not  
249 decrease with methylene blue concentration, as reported for methanol (45) but contrary to  
250 what is generally observed in water (46). Thus, dimer formation is not favored by high  
251 concentrations of methylene blue. In the presence of oxygen and phospholipids, methylene  
252 blue gradually loses its color in visible light, resulting in a completely colorless solution.  
253 However, at high methylene blue concentrations and large solution volumes, the methylene  
254 blue was degraded only very slightly, with absorbance values remaining high from 220 nm to  
255 340 nm (UV) and from 540 to 700 nm. For absorbance at 654 nm (characteristic wavelength  
256 of methylene blue illumination for singlet oxygen generation) and different path lengths,  
257 99.9% of the light at this wavelength was found to have been absorbed after a path length of  
258 only 1 mm, so almost 90% of the sample received no illumination (see supplementary  
259 information).

260 Similar qualitative behavior was observed for the mass extinction coefficient at 233 nm  
261 (Proba.1 < 0.01, Proba.2 =0.059), the two responses being highly correlated (table 6). Indeed,  
262 the presence of conjugated dienes is directly related to the amount of hydroperoxide formed  
263 (fig. 2b). This amount did not decrease within the limits of the experimental design, implying  
264 that conjugated dienes were not significantly degraded through oxidative scission.

265 For comparison, the unilluminated sample (covered with a sheet of aluminum foil) had a low  
266 extinction coefficient ( $0.279 \text{ L.g}^{-1}.\text{cm}^{-1}$ ).

### 267 **3.2.2. Extinction coefficient ratio**



268 The ratio of extinction coefficients at 233 nm/270 nm was described by the model with a  
269 better validity than extinction at 233 nm (Proba.1 = 0.033, Proba.2 = 71.9) and its behavior  
270 was different (fig. 3). The equation with coded values for log(1/V) and log(C) can be written:

$$\begin{aligned} 271 \quad \epsilon_{233\text{nm}/270\text{nm}} &= 32.31 + 6.11 \times \log(1/V) - 11.07 \times \log C_{\text{MB}} - 10.56 \times [\log(1/V)]^2 - 14.81 \times [\log C_{\text{MB}}]^2 + \\ 272 \quad &8.81 \times \log(1/V) \times \log C_{\text{MB}} \end{aligned}$$

$$273 \quad R^2 = 0.991$$

274 The model could therefore be considered valid for the experimental points used to determine  
275 the coefficients, but it was also necessary to check the test points (table 5).

276 The results for the test points indicated that low extinction ratios displayed greater deviations  
277 from the model, and two calculated values (experiments 11 and 13) were significantly  
278 different from the experimental values. The model was found to have a high descriptive and  
279 moderate predictive value.

280 The equation confirms that the extinction ratio is inversely correlated with methylene blue  
281 concentration (see also table 6). Extinction at 270 nm can be considered characteristic of  
282 conjugated trienes, and the change in extinction ratio from poorly to strongly oxidative  
283 conditions indicates that these molecules are readily obtained in extreme conditions, with the  
284 lowest ratio obtained for a low air volume and high methylene blue concentration. It could be  
285 hypothesized that, as only the methylene blue close to the surface is illuminated, these  
286 conditions result in a high concentration of singlet oxygen in a small volume. Surface  
287 phospholipids are, thus, strongly oxidized, whereas molecules located at deeper positions in  
288 the solution are not. Increasing oxygen levels result in greater methylene blue degradation,  
289 resulting in the gradual illumination of the entire sample and a homogenization of oxidation  
290 mechanisms.

291 **Size and zeta potential of vesicles**

292 The size of the vesicles formed was determined by drying 1 mL of the phospholipid solution  
293 under N<sub>2</sub>, adding 2 mL of deionized water and sonicating the sample for three minutes in  
294 pulse mode (5 s ON/10 s OFF). Vesicles were then analyzed by measuring dynamic light  
295 scattering (DLS) (table 5).

296 The Z-average value gives the intensity-weighted harmonic mean size. As this variable was  
297 the most stable (see supplementary information), it is selected as the response variable. In  
298 terms of mean size, structures smaller than 10 nm across were measured, which may have  
299 resulted from the association of a very small number of phospholipids. Based on the size  
300 ranges obtained, ultrasonication seems to generate mostly small unilamellar liposomes (47).

301 The statistical analysis showed that the model obtained for Z-average size was both  
302 significant (Proba.1 < 0.01) and valid (Proba.2 =31.9) .

303 The equation for the Z-average size of vesicles was:

$$304 \quad Z = 237 - 101 \times \log(1/V) - 166 \times \log C_{MB} + 4 \times [\log(1/V)]^2 + 45 \times [\log C_{MB}]^2 +$$
$$305 \quad 121 \times \log(1/V) \times \log C_{MB}$$

$$306 \quad R^2 = 0.997$$

307 Mean size was not correlated with yield, but was inversely correlated with methylene blue  
308 concentration (table 6), as small vesicles were obtained at high methylene blue  
309 concentrations, even with only low levels of oxidation. The large decrease in average size  
310 with increasing methylene blue concentration and phospholipid solution volume can be  
311 deduced from the equation and observed on the response surface (fig. 4).

312 However, due to the instability of some vesicle solutions, the test points gave values either  
313 lower than those calculated by the model. The smaller size of the vesicles in oxidized samples  
314 may result from mechanical destabilization of the vesicles due to oxidation (48), leading to a  
315 partial rupture of vesicles, but it may also indicate that membrane formation requires less  
316 energy with oxidized than with native phospholipids. Indeed, increasing the polarity of the

317 fatty acid chains of phospholipids decreases the interaction energy between water and  
318 phospholipids. At high concentrations of methylene blue, the volume of solution had a lesser  
319 effect. Even if the volume of air is small, a high concentration of methylene blue allows the  
320 formation of small vesicles. Despite its presence at a molar concentration well below that of  
321 phospholipids ( $1 \text{ mM} \ll \sim 25 \text{ mM}$ ), methylene blue may make a non-negligible contribution  
322 to the surface properties of vesicles. As this compound is positively charged, a measurement  
323 of the zeta potential of the vesicle solutions is likely to be informative.

324 Zeta potential can be related to the surface charge of vesicles. The analysis of variance  
325 revealed the experimental design to be highly significant (Proba.1 =0.867), whereas the  
326 validity of the quadratic model was slightly low (Proba.2 =3.46).

327 If the membrane surface consisted solely of the polar heads of phospholipids, then low,  
328 mostly negative zeta potentials would be observed, as for vesicles formed without methylene  
329 blue and with unoxidized soybean PC only (zeta potential of  $-8.66 \pm 0.42 \text{ mV } N=3$ ). The  
330 negativity of the zeta potential in this context is accounted for by the more favorable exposure  
331 of the phosphate group than of the choline group (49, 50). When methylene blue is present at  
332 a high concentration, without consumption due to a high oxygen level, then zeta potential is  
333 positive (fig. 5). This potential can reach values of more than 40 mV and can therefore induce  
334 strong electrostatic repulsions between vesicles, limiting aggregation, potentially accounting  
335 for the smaller sizes observed. Zeta potential is negative when methylene blue concentration  
336 is high but solution volume is low, due to the consumption of methylene blue. Indeed, the  
337 degradation of methylene blue under oxidative conditions leads to a loss of its charge (51, 52).  
338 This strong contribution of methylene blue to zeta potential, as confirmed by the high  
339 correlation coefficient (table 6), results in its positioning at the surface of vesicles, close to the  
340 phospholipids, accounting for its preferential reaction with phospholipids rather than with  
341 fatty acids. As a cationic molecule, methylene blue adsorbs onto the zwitterionic surface and  
342 may change the orientation of the P-N dipole, tilting it away (53). This may increase the  
343 expression of the positive charge carried by the choline group. More surprisingly, positive

344 zeta potentials were also observed in the presence of low methylene blue concentrations and  
345 small solution volumes. In small volumes, methylene blue is totally degraded and zeta  
346 potential depends principally on the conformation of the phosphatidylcholine group. The  
347 orientation of the phosphocholine group at the membrane surface may depend on ionic  
348 strength(50). Conductivity increases with increasing methylene blue concentration (from  
349 about 0.01 mS/cm to 0.1 mS/cm), but the anionic charge on phosphatidyl groups should be  
350 more strongly expressed at low concentrations. Oxidation allows more polar fatty acid chains  
351 to move toward the external aqueous phase (54, 55), potentially interacting with anionic  
352 phosphate groups. Hydroperoxidized fatty acid chains seem to remain in the membrane core  
353 (56). Thus, in the absence of photosensitization, oxidation may generate more diverse  
354 products interacting preferentially with the phosphate group.

### 355 **3.2.3. Permeation studies**

356 KCl is a salt known to permeate liposomes less efficiently than water (10). Changes in the  
357 size of liposomes formed from unoxidized phospholipids are therefore more likely to be due  
358 to water fluxes than to the movement of KCl. When a solution of vesicles formed with pure  
359 dilinoleylphosphatidylcholine (DLiPC) in 0.1 M KCl is dispersed in 2 M KCl, absorbance  
360 initially increases considerably, due to light scattering by vesicles. The vesicles are far less  
361 permeable to KCl than to water, so water efflux occurs and the vesicle shrinks. An increase in  
362 absorbance is observed over recording times of more than 5 s ( $Abs_0 - Abs_{eq.} = -0.072 \pm 0.001$  ;  
363  $Abs_{eq.} = 0.585 \pm 0.028$ ). A similar absorbance profile is obtained with soybean  
364 phosphatidylcholine, but with a lower absorbance and less pronounced variation, suggesting a  
365 lower permeability of these vesicles to water (see supplementary information). The main  
366 barrier to permeation is generally the highest ordered section of the bilayer. Unsaturation  
367 leads to lower chain-ordering values and an increase in membrane fluidity, potentially leading  
368 to transient defects or pores, increasing water permeation. Soybean phosphatidylcholine cans  
369 fewer unsaturated bonds and is therefore, less permeable to water (5–7).

370 The absorbance of many samples did not change significantly over the time course of the  
371 permeation test, making it impossible to model the  $\Delta A$  parameter correctly. However, certain  
372 types of behavior emerged. The sample corresponding to experiment 14 (tables 4 and 5)  
373 oxidized with the lowest methylene blue concentration and a small volume of air, with a low  
374 extinction coefficient at 233 nm and a yield (2.72 and 16.25%, respectively) similar to that for  
375 soybean PC. Vesicles formed with phospholipids oxidized at the lowest methylene blue  
376 concentration and a medium-high air volume mostly displayed a decrease in absorbance over  
377 time (samples 4, 5 and 12), indicating swelling and an increase in KCl permeation. Samples  
378 with medium-high methylene blue concentrations but low air volumes (2 and 13) formed  
379 small vesicles with a high absorbance that increased over time, indicating shrinkage due to  
380 water efflux. This high absorbance may also be partly due to the presence of unconsumed  
381 methylene blue rather than purely the result of scattering. Phospholipids oxidized with  
382 medium-high air volumes and medium-high methylene blue concentrations (samples 1, 3, 7,  
383 8, 9, 11), which have had extinction coefficients at 233 nm ( $>8 \text{ L}\cdot\text{g}^{-1}\cdot\text{cm}^{-1}$ ), formed vesicle  
384 suspensions with a low absorbance that did not vary over time, indicative of a total absence of  
385 swelling/shrinkage behavior. This low absorbance can be linked to the small size of the  
386 vesicles and the absence of variation may be due to the high level of membrane permeability,  
387 as also observed for samples 6 and 10. This behavior, despite low hydroperoxide yields and  
388 low 233 nm extinction ratios, may be due to the high concentration of methylene blue,  
389 suggesting that this molecule can promote membrane permeability in the presence of low-  
390 level oxidation. The surface response corresponding to the final absorbance  $A_{\text{inf}}$  (fig. 6) can be  
391 obtained, to assess the extent to which it is linked to initial vesicle size or methylene blue  
392 concentration. Statistical analysis showed the model to be highly significant (Proba.1  $<0.01$ ),  
393 with good validity (Proba.2 =84.1).

394 The equation determined for final absorbance was:

$$395 A_{\text{inf}} = 0.161 - 0.149 \times \log(1/V) + 0.021 \times \log C_{\text{MB}} + 0.100 \times [\log(1/V)]^2 + 0.071 \times [\log C_{\text{MB}}]^2 -$$
$$396 0.0102 \times \log(1/V) \times \log C_{\text{MB}}$$

397  $R^2 = 0.996$

398 The test points displayed only limited divergence from the calculated values, so the model  
399 describes experimental values well, but also has predictive power. This predictive power  
400 could be improved by increasing the degrees of freedom. The shape of the response surface  
401 was different from that for vesicle size (fig. 6). Even if the positive contribution of methylene  
402 blue to absorbance must be taken into account, this figure, the equation above and table 6  
403 indicate that final absorbance is correlated principally with solution volume, whereas vesicle  
404 size is essentially inversely correlated with methylene blue concentration. Both yield and  
405 extinction coefficients are inversely correlated with final absorbance, and are therefore not  
406 entirely dependent on initial size but on the hydroperoxide content of the phospholipids  
407 forming the vesicle membrane, determining its ability to swell/shrink.

#### 408 **4. Conclusion**

409 Methylene blue favored interaction with soybean phospholipids. Used as a tool for monitoring  
410 the photosensitized oxidation of phospholipids, methylene blue could improve our  
411 understanding of membrane modifications at low to medium levels of oxidation. Its influence  
412 on the surface charge and size of phospholipid vesicles can be controlled through response  
413 surface methods and could be used to adapt the stability and transport properties of liposomes.

#### 414 **Author Contribution section**

415 J-F. F. designed and performed research, analyzed data and wrote the manuscript.

416 M. C. contributed analytical tools, analyzed data.

417 A. C. contributed analytical tools, analyzed data.

418 Z. M. designed research, analyzed data.

#### 419 **Acknowledgments**

420 The authors thank the Occitanie region for financial support through the SMON-FERT  
421 RECH project, grant no. 1405981.

422 The authors thank Mr. Marc Vedrenne of the University of Toulouse for assistance with NMR  
423 analysis and Dr Aurélie BEAL and Prof. Roger PHAN TAN LUU from NEMRODOW for  
424 scientific assistance.

425 **Supporting information:** One file containing statistical processing tables of the experimental  
426 design, details of NMR analysis, absorbance variations of methylene blue solutions with  
427 concentration and path length, details of dynamic light scattering measurements and  
428 permeation studies.

## 429 **References**

- 430 1. Allen, T.M., and P.R. Cullis. 2013. Liposomal drug delivery systems: From concept to  
431 clinical applications. *Adv. Drug Deliv. Rev.* 65: 36–48.
- 432 2. Bozzuto, G., and A. Molinari. 2015. Liposomes as nanomedical devices. *Int. J.*  
433 *Nanomedicine.* : 975.
- 434 3. Li, J., X. Wang, T. Zhang, C. Wang, Z. Huang, X. Luo, and Y. Deng. 2015. A review on  
435 phospholipids and their main applications in drug delivery systems. *Asian J. Pharm. Sci.*  
436 10: 81–98.
- 437 4. Akizuki, H., and T. Kaneko. 2016. Characteristics of liposomes made by  
438 phosphatidylethanolamine. *Biophys. J.* 110: 71a.
- 439 5. Bittman, R., and L. Blau. 1972. Phospholipid-cholesterol interaction. Kinetics of water  
440 permeability in liposomes. *Biochemistry (Mosc.)*. 11: 4831–4839.
- 441 6. De Gier, J., J.G. Mandersloot, and L.L.M. Van Deenen. 1968. Lipid composition and  
442 permeability of liposomes. *Biochim. Biophys. Acta BBA - Biomembr.* 150: 666–675.
- 443 7. Olbrich, K., W. Rawicz, D. Needham, and E. Evans. 2000. Water permeability and  
444 mechanical strength of polyunsaturated lipid bilayers. *Biophys. J.* 79: 321–327.
- 445 8. Barton, P.G., and F.D. Gunstone. 1975. Hydrocarbon chain packing and molecular  
446 motion in phospholipid bilayers formed from unsaturated lecithins. Synthesis and  
447 properties of sixteen positional isomers of 1,2-dioctadecenoyl-sn-glycero-3-  
448 phosphorylcholine. *J. Biol. Chem.* 250: 4470–4476.
- 449 9. Blok, M.C., E.C.M. Van Der Neut-Kok, L.L.M. Van Deenen, and J. De Gier. 1975. The  
450 effect of chain length and lipid phase transitions on the selective permeability properties  
451 of liposomes. *Biochim. Biophys. Acta BBA - Biomembr.* 406: 187–196.
- 452 10. Paula, S., A.G. Volkov, A.N. Van Hoek, T.H. Haines, and D.W. Deamer. 1996.  
453 Permeation of protons, potassium ions, and small polar molecules through phospholipid  
454 bilayers as a function of membrane thickness. *Biophys. J.* 70: 339–348.
- 455 11. Kotova, E.A., A.V. Kuzevanov, A.A. Pashkovskaya, and Y.N. Antonenko. 2011.  
456 Selective permeabilization of lipid membranes by photodynamic action via formation of

- 457 hydrophobic defects or pre-pores. *Biochim. Biophys. Acta BBA - Biomembr.* 1808:  
458 2252–2257.
- 459 12. Jurkiewicz, P., A. Olżyńska, L. Cwiklik, E. Conte, P. Jungwirth, F.M. Megli, and M.  
460 Hof. 2012. Biophysics of lipid bilayers containing oxidatively modified phospholipids:  
461 Insights from fluorescence and EPR experiments and from MD simulations. *Biochim.*  
462 *Biophys. Acta BBA - Biomembr.* 1818: 2388–2402.
- 463 13. Tanfani, F., and E. Bertoli. 1989. Permeability of oxidized phosphatidylcholine  
464 liposomes. *Biochem. Biophys. Res. Commun.* 163: 241–246.
- 465 14. Lis, M., A. Wizert, M. Przybylo, M. Langner, J. Swiatek, P. Jungwirth, and L. Cwiklik.  
466 2011. The effect of lipid oxidation on the water permeability of phospholipids bilayers.  
467 *Phys. Chem. Chem. Phys.* 13: 17555.
- 468 15. Smolen, J.E., and Shohet, Stephen B. 1974. Permeability changes induced by  
469 peroxidation in liposomes prepared from human erythrocyte lipids. *J. Lipid Res.* 15:  
470 273–280.
- 471 16. Runas, K.A., and N. Malmstadt. 2015. Low levels of lipid oxidation radically increase  
472 the passive permeability of lipid bilayers. *Soft Matter.* 11: 499–505.
- 473 17. Van der Paal, J., E.C. Neyts, C.C.W. Verlackt, and A. Bogaerts. 2016. Effect of lipid  
474 peroxidation on membrane permeability of cancer and normal cells subjected to  
475 oxidative stress. *Chem Sci.* 7: 489–498.
- 476 18. Itri, R., H.C. Junqueira, O. Mertins, and M.S. Baptista. 2014. Membrane changes under  
477 oxidative stress: the impact of oxidized lipids. *Biophys. Rev.* 6: 47–61.
- 478 19. Mertins, O., I.O.L. Bacellar, F. Thalmann, C.M. Marques, M.S. Baptista, and R. Itri.  
479 2014. Physical damage on giant vesicles membrane as a result of methylene blue  
480 photoirradiation. *Biophys. J.* 106: 162–171.
- 481 20. Megli, F.M., L. Russo, and E. Conte. 2009. Spin labeling EPR studies of the properties  
482 of oxidized phospholipid-containing lipid vesicles. *Biochim. Biophys. Acta BBA -*  
483 *Biomembr.* 1788: 371–379.
- 484 21. Memoli, A., L.G. Palermiti, V. Travagli, and F. Alhaique. 1996. Studies of differently  
485 induced peroxidation phenomena in lecithins. *J. Agric. Food Chem.* 44: 2814–2817.
- 486 22. Reis, A., and C.M. Spickett. 2012. Chemistry of phospholipid oxidation. *Oxidized*  
487 *Phospholipids - Their Prop. Interact. Proteins.* 1818: 2374–2387.
- 488 23. Aubry, J.M., and B. Cazin. 1988. Chemical sources of singlet oxygen. 2. Quantitative  
489 generation of singlet oxygen from hydrogen peroxide disproportionation catalyzed by  
490 molybdate ions. *Inorg. Chem.* 27: 2013–2014.
- 491 24. Boehme, K., and H.D. Brauer. 1992. Generation of singlet oxygen from hydrogen  
492 peroxide disproportionation catalyzed by molybdate ions. *Inorg. Chem.* 31: 3468–3471.
- 493 25. Watabe, N., Y. Ishida, A. Ochiai, Y. Tokuoka, and N. Kawashima. 2007. Oxidation  
494 decomposition of unsaturated fatty acids by singlet oxygen in phospholipid bilayer  
495 membranes. *J. Oleo Sci.* 56: 73–80.



- 496 26. Eisenberg, W. C.; Anand, J.; Wang, S.; Stevenson, R. J. Oxidation of  
497 phosphatidylcholine membranes by singlet oxygen generated in the gas phase.  
498 *Photochem. Photobiol.* **1992**, *56* (4), 441–445.
- 499 27. Hackbarth, S., and B. Röder. 2015. Singlet oxygen luminescence kinetics in a  
500 heterogeneous environment – identification of the photosensitizer localization in small  
501 unilamellar vesicles. *Photochem Photobiol Sci.* *14*: 329–334.
- 502 28. Abrahamse, H., and M.R. Hamblin. 2016. New photosensitizers for photodynamic  
503 therapy. *Biochem. J.* *473*: 347–364.
- 504 (29) Chacon, J. N.; McLearn, J.; Sinclair, R. S. Singlet oxygen yields and radical  
505 contributions in the dye-sensitized photo-oxidation in methanol of esters of  
506 polyunsaturated fatty acids (oleic, linoleic, linolenic and arachidonic). *Photochem.*  
507 *Photobiol.* **1988**, *47* (5), 647–656.
- 508 30. Terao, J., Y. Hirota, M. Kawakatsu, and S. Matsushita. 1981. Structural analysis of  
509 hydroperoxides formed by oxidation of phosphatidylcholine with singlet oxygen. *Lipids.*  
510 *16*: 427–432.
- 511 31. Jiang, J., and A. Kamal-Eldin. 1998. Comparing methylene blue-photosensitized  
512 oxidation of methyl-conjugated linoleate and methyl linoleate. *J. Agric. Food Chem.* *46*:  
513 923–927.
- 514 32. Hilarius, P.M., I.G. Ebbing, D.W.C. Dekkers, J.W.M. Lagerberg, D. de Korte, and A.J.  
515 Verhoeven. 2004. Generation of singlet oxygen induces phospholipid scrambling in  
516 human erythrocytes. *Biochemistry (Mosc.)*. *43*: 4012–4019.
- 517 33. DeRosa, M. 2002. Photosensitized singlet oxygen and its applications. *Coord. Chem.*  
518 *Rev.* *233–234*: 351–371.
- 519 34. Nowell, N.H., H.-I. Hung, L.A. Austin, and C.L. Evans. 2016. EtNBS in photodynamic  
520 therapy. In: *Handbook of Photodynamic Therapy. Updates on Recent Applications of*  
521 *Porphyrin-Based Compounds.* Ravindra K Pandey , David Kessel, Thomas J. Dougherty.  
522 pp. 365–380.
- 523 35. de Souza, R.M., P. Siani, T.F. Schmidt, R. Itri, and L.G. Dias. 2017. Methylene blue  
524 location in (hydroperoxidized) cardiolipin monolayer: implication in membrane  
525 photodegradation. *J. Phys. Chem. B.* *121*: 8512–8522.
- 526 36. Roche, J., A. Bouniols, Z. Mouloungui, T. Barranco, and M. Cerny. 2006. Management  
527 of environmental crop conditions to produce useful sunflower oil components. *Eur. J.*  
528 *Lipid Sci. Technol.* *108*: 287–297.
- 529 37. Ardhammar, M., P. Lincoln, and B. Nordén. 2002. Invisible liposomes: Refractive index  
530 matching with sucrose enables flow dichroism assessment of peptide orientation in lipid  
531 vesicle membrane. *Proc. Natl. Acad. Sci. USA* *99*: 15313–15317.
- 532 38. Mie, G. 1908. Beiträge zur Optik trüber Medien, speziell kolloidaler Metallösungen.  
533 *Ann. Phys.* *330*: 377–445.
- 534 39. Ghosh, P., and U.N. Singh. 1992. Liposome shrinkage and swelling under osmotic-  
535 diffusional stress: evaluation of kinetic parameters from spectrophotometric  
536 measurements. *Biochim. Biophys. Acta BBA - Biomembr.* *1110*: 88–96.

- 537 40. Knothe, G., and J.A. Kenar. 2004. Determination of the fatty acid profile by <sup>1</sup>H-NMR  
538 spectroscopy. *Eur. J. Lipid Sci. Technol.* 106: 88–96.
- 539 41. Kim, W., H. Rho, Y. Hong, M. Yeom, S. Shin, J. Yi, M.-S. Lee, H. Park, and D. Cho.  
540 2013. Determination and comparison of seed oil triacylglycerol composition of various  
541 soybeans (*Glycine max* (L.)) using <sup>1</sup>H-NMR spectroscopy. *Molecules.* 18: 14448–  
542 14454.
- 543 42. Gardner, H.W., and D. Weisleder. 1972. Hydroperoxides from oxidation of linoleic and  
544 linolenic acids by soybean lipoxygenase: Proof of the trans-11 double bond. *Lipids.* 7:  
545 191–193.
- 546 43. Neff, W.E., E.N. Frankel, and K. Miyashita. 1990. Autoxidation of polyunsaturated  
547 triacylglycerols. I. Trilinoleoylglycerol. *Lipids.* 25: 33–39.
- 548 44. Porter, N.A., and J.S. Wujek. 1987. Allylic hydroperoxide rearrangement: Beta-scission  
549 or concerted pathway? *J. Org. Chem.* 52: 5085–5089.
- 550 45. Zhao, Z., and E.R. Malinowski. 1999. Determination of the hydration of methylene blue  
551 aggregates and their dissociation constants using visible spectroscopy. *Appl. Spectrosc.*  
552 53: 1567–1574.
- 553 46. Morgounova, E., Q. Shao, B.J. Hackel, D.D. Thomas, and S. Ashkenazi. 2013.  
554 Photoacoustic lifetime contrast between methylene blue monomers and self-quenched  
555 dimers as a model for dual-labeled activatable probes. *J. Biomed. Opt.* 18: 056004.
- 556 47. Akbarzadeh, A., R. Rezaei-Sadabady, S. Davaran, S.W. Joo, N. Zarghami, Y.  
557 Hanifehpour, M. Samiei, M. Kouhi, and K. Nejati-Koshki. 2013. Liposome:  
558 classification, preparation, and applications. *Nanoscale Res. Lett.* 8: 102.
- 559 48. Makky, A., and M. Tanaka. 2015. Impact of lipid oxidization on biophysical properties  
560 of model cell membranes. *J. Phys. Chem. B.* 119: 5857–5863.
- 561 49. Chibowski, E., and A. Szczeń. 2016. Zeta potential and surface charge of DPPC and  
562 DOPC liposomes in the presence of PLC enzyme. *Adsorption.* 22: 755–765.
- 563 50. Makino, K., T. Yamada, M. Kimura, T. Oka, H. Ohshima, and T. Kondo. 1991.  
564 Temperature- and ionic strength-induced conformational changes in the lipid head group  
565 region of liposomes as suggested by zeta potential data. *Biophys. Chem.* 41: 175–183.
- 566 51. Dariani, R.S., A. Esmaeili, A. Mortezaali, and S. Dehghanpour. 2016. Photocatalytic  
567 reaction and degradation of methylene blue on TiO<sub>2</sub> nano-sized particles. *Opt. - Int. J.*  
568 *Light Electron Opt.* 127: 7143–7154.
- 569 52. Houas, A. 2001. Photocatalytic degradation pathway of methylene blue in water. *Appl.*  
570 *Catal. B Environ.* 31: 145–157.
- 571 53. Haugen, A., and S. May. 2007. The influence of zwitterionic lipids on the electrostatic  
572 adsorption of macroions onto mixed lipid membranes. *J. Chem. Phys.* 127: 215104.
- 573 54. Khandelia, H., and O.G. Mouritsen. 2009. Lipid gymnastics: evidence of complete acyl  
574 chain reversal in oxidized phospholipids from molecular simulations. *Biophys. J.* 96:  
575 2734–2743.

- 576 55. Sabatini, K., J.-P. Mattila, F.M. Megli, and P.K.J. Kinnunen. 2006. Characterization of  
577 two oxidatively modified phospholipids in mixed monolayers with DPPC. *Biophys. J.*  
578 90: 4488–4499.
- 579 56. Siani, P., R.M. de Souza, L.G. Dias, R. Itri, and H. Khandelia. An overview of molecular  
580 dynamics simulations of oxidized lipid systems, with a comparison of ELBA and  
581 MARTINI force fields for coarse grained lipid simulations. *Biochim. Biophys. Acta*  
582 BBA - Biomembr. 10: 2498-2511
- 583

584 Figure 1. Difference between the  $^1\text{H}$ -NMR spectra of soybean phosphatidylcholine and  
585 oxidized phosphatidylcholine (the spectra have been truncated to highlight the main  
586 differences between them)

587 Figure 2. a) Response surface representation for hydroperoxide yield. b) Response surface  
588 representation for the extinction coefficient at 233 nm

589 Figure 3. Response surface representation for the ratio of extinction coefficients.

590 Figure 4. Response surface representation for the Z-average size of vesicles (in nm)

591 Figure 5. Response surface representation for the zeta potential of vesicles

592 Figure 6. Response surface representation for the final absorbance of vesicles

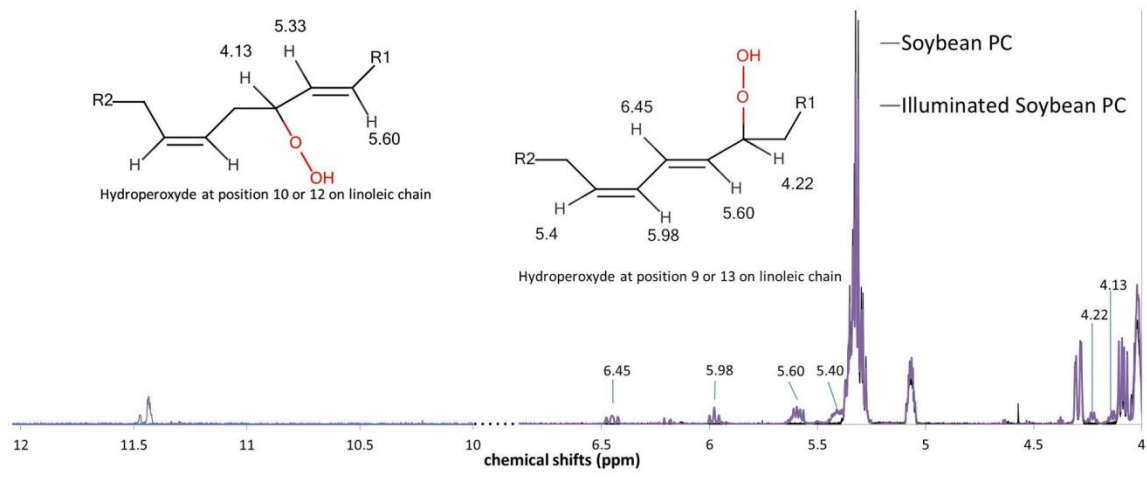
593

594

595

596

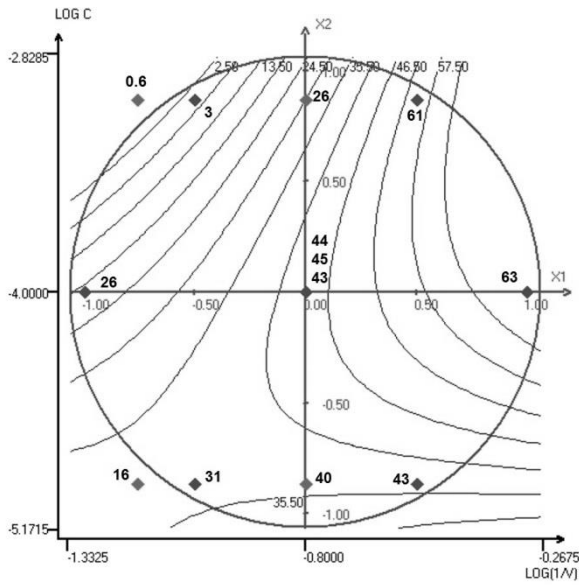
597



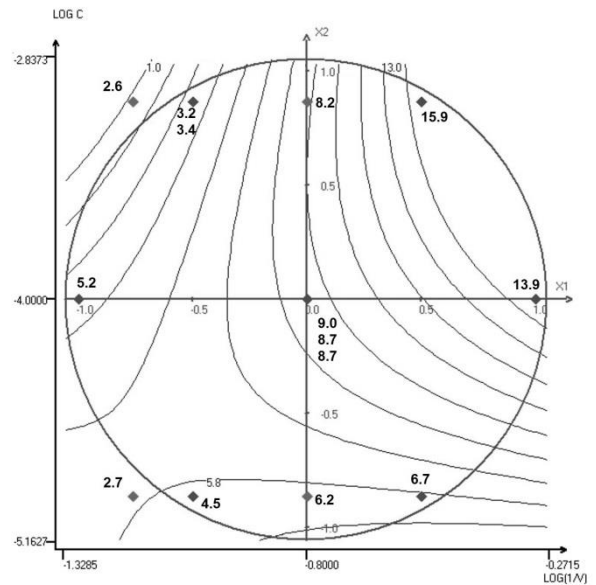
598

599

600

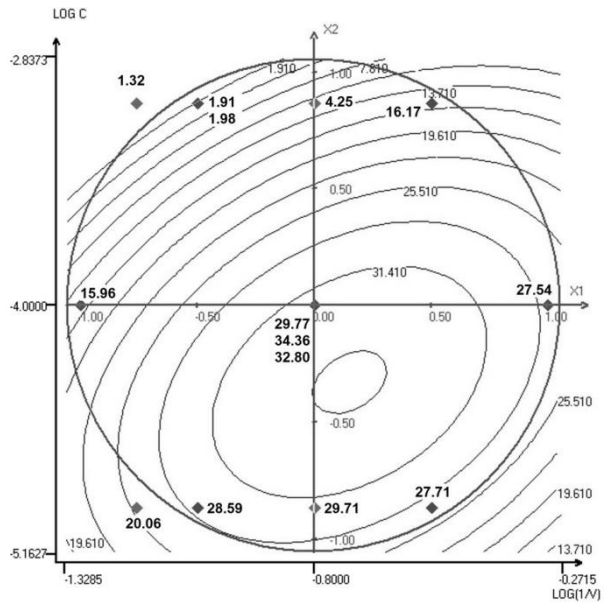


a



b

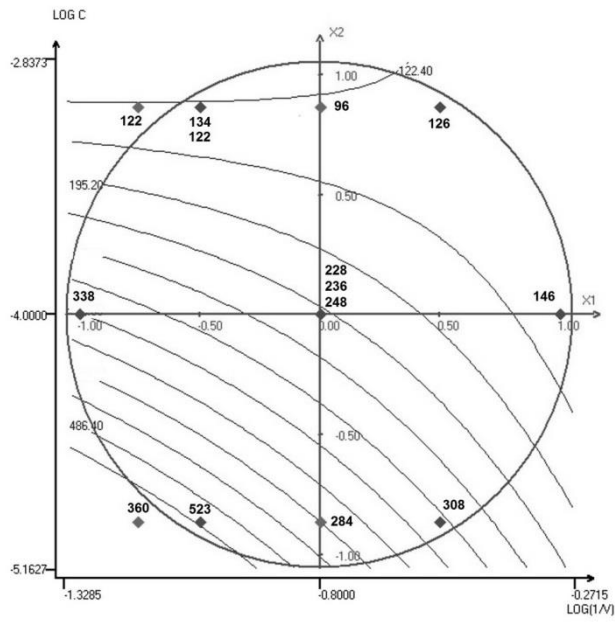
Note : Experimental points are situated in the figure with their experimental values.



602

603

604

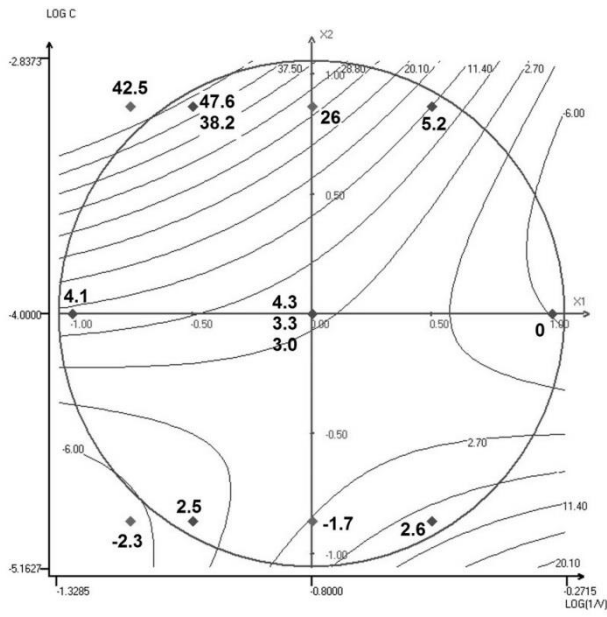


605

606



607



608

